Early Science
High Speed Combustion and Detonation Project (HSCD)

Alexei Khokhlov, University of Chicago
Joanna Austin, University of Illinois
Andrew Knisely, University of Illinois
Katherine Riley, ANL
Charles Bacon, ANL
Ben Clifford, ANL
Shashi Aithal, ANL
Marta Garcia, ANL

Overview

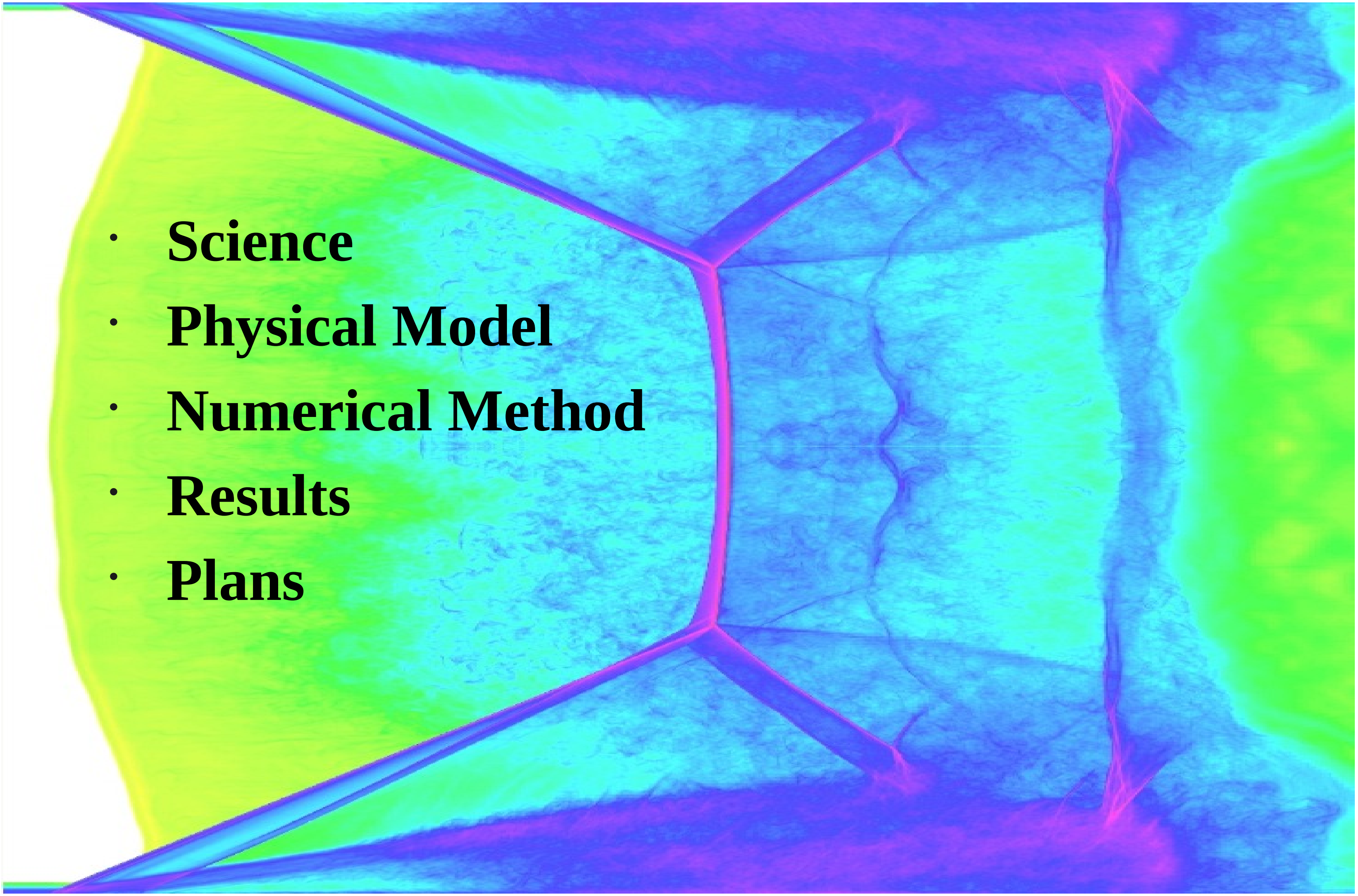

- **Science**
- **Physical Model**
- **Numerical Method**
- **Results**
- **Plans**

High speed combustion

Reactive flows with velocities ~ sound speed.

- chemical reactions
- viscosity
- heat conduction
- diffusion of chemical species
- fluid instabilities
- boundary layers
- turbulence
- radiation
- <u>compressibility</u>
- <u>shocks</u>

All processes are coupled.
Range of physical scales.
Flow is rapidly evolving.

Combustion experiments in shock tubes

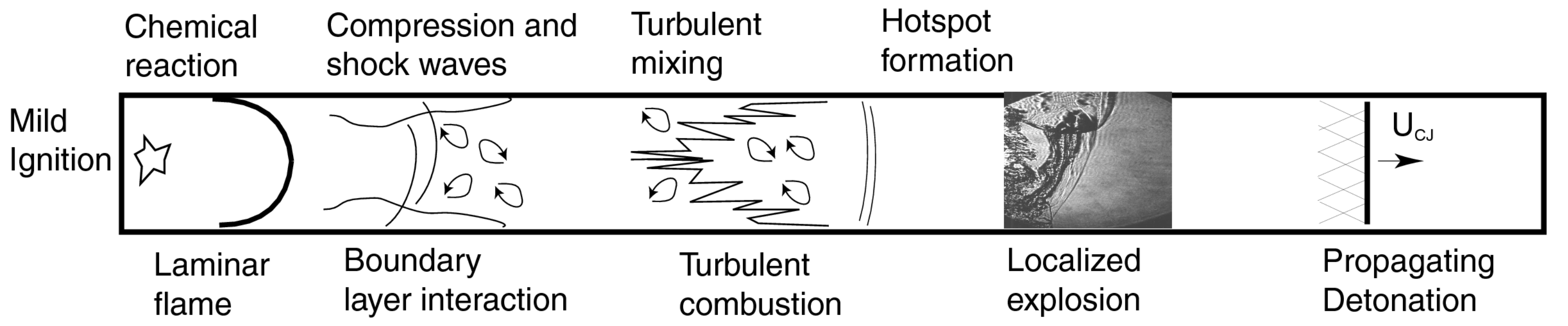

Flame,
Deflagration-to-detonation transition (DDT)
Detonation

Accelerating turbulent flame

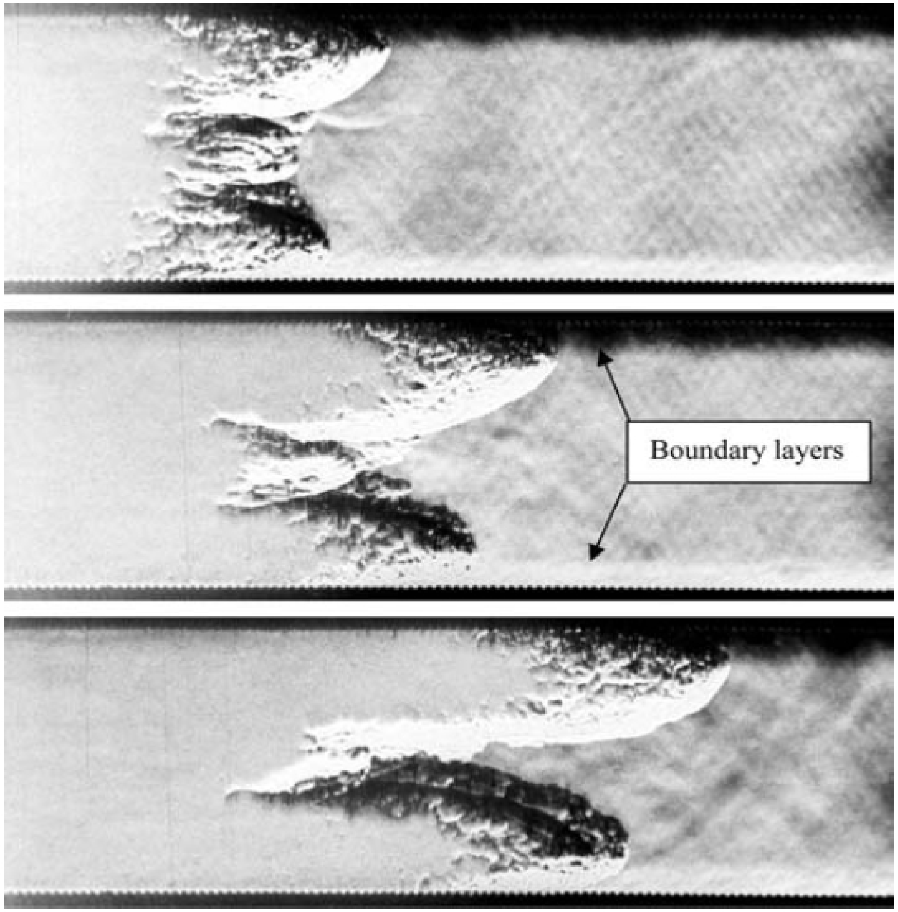

Fig. 10 Sequence of shadow photographs (0.1 ms between frames) showing boundary layers ahead of accelerated flame. Flame propagates from left to right; speed of lead flame edges is about 320 m/s. Boundary layers are seen as dark regions on the top wall and as lighter regions in the bottom wall of the channel. Wall roughness is 1 mm; mixture is stoichiometric H_2–O_2 at initial pressure of 0.6 bar

Kyznetsov 2005

Detonation

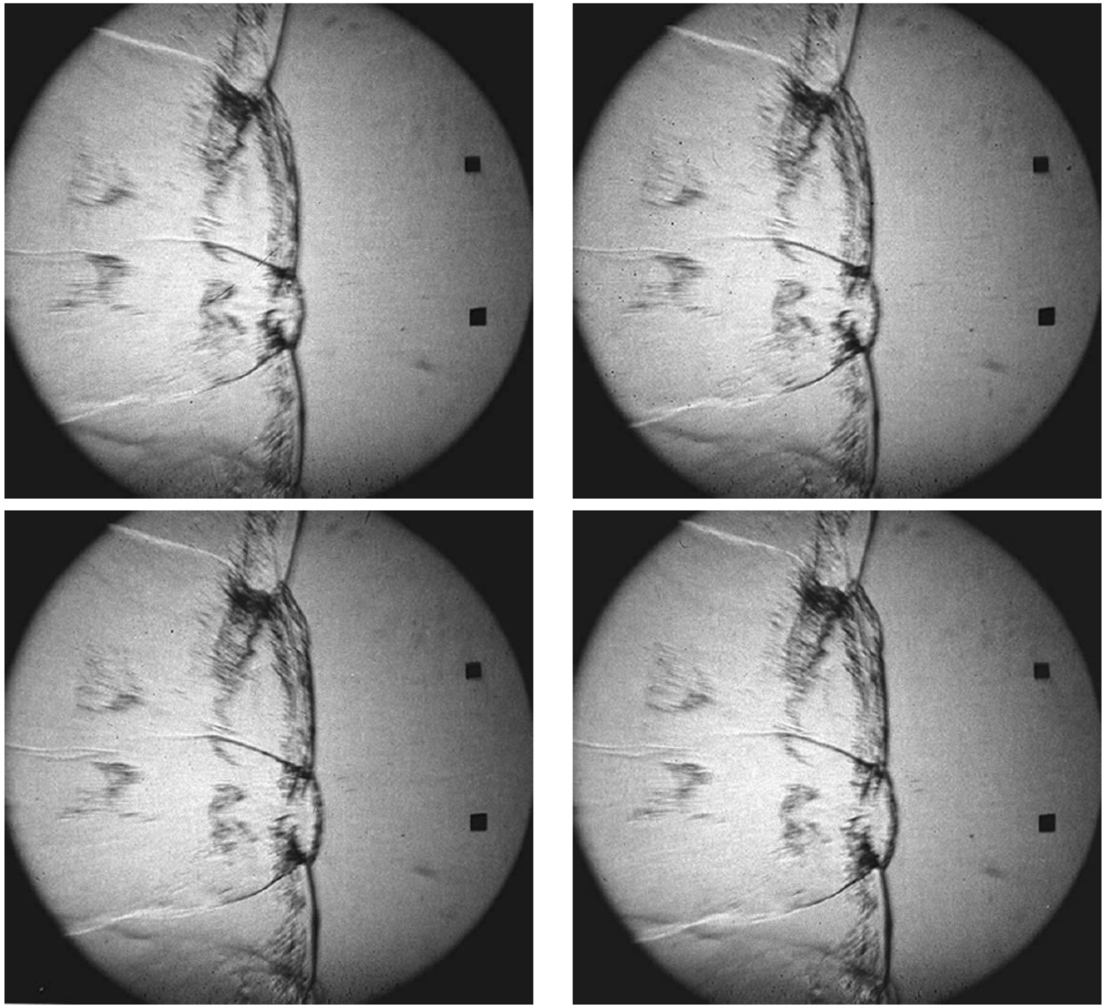

Austin 2001

Defalgration-to-detonation transition (DDT)

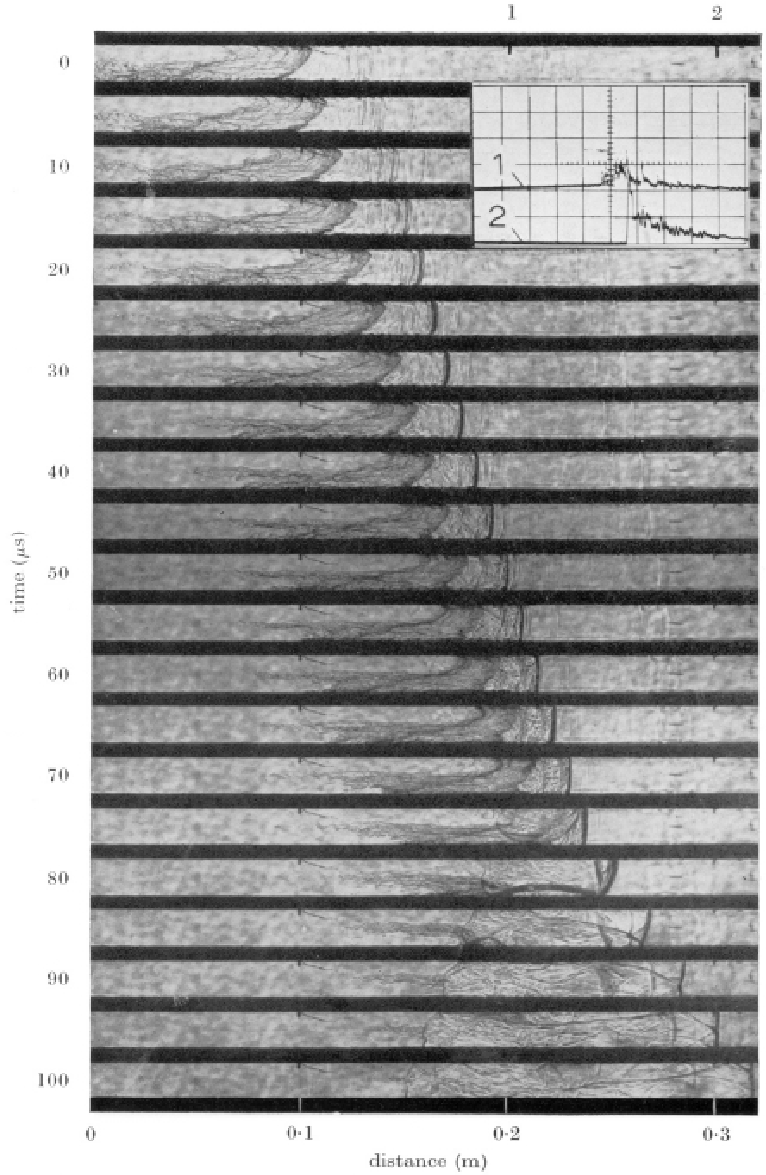

Figure 6. Stroboscopic schlieren record of the transition to detonation with onset between flame and shock. $2H_2 + O_2$ initially at a pressure of 554 mmHg. Pressure record shown in insert. Vertical scale: 1 division = 200 Lb./in.². Horizontal scale: 1 division = 50 μs. Oscilloscope sweep leads the photographic record by 180 μs.

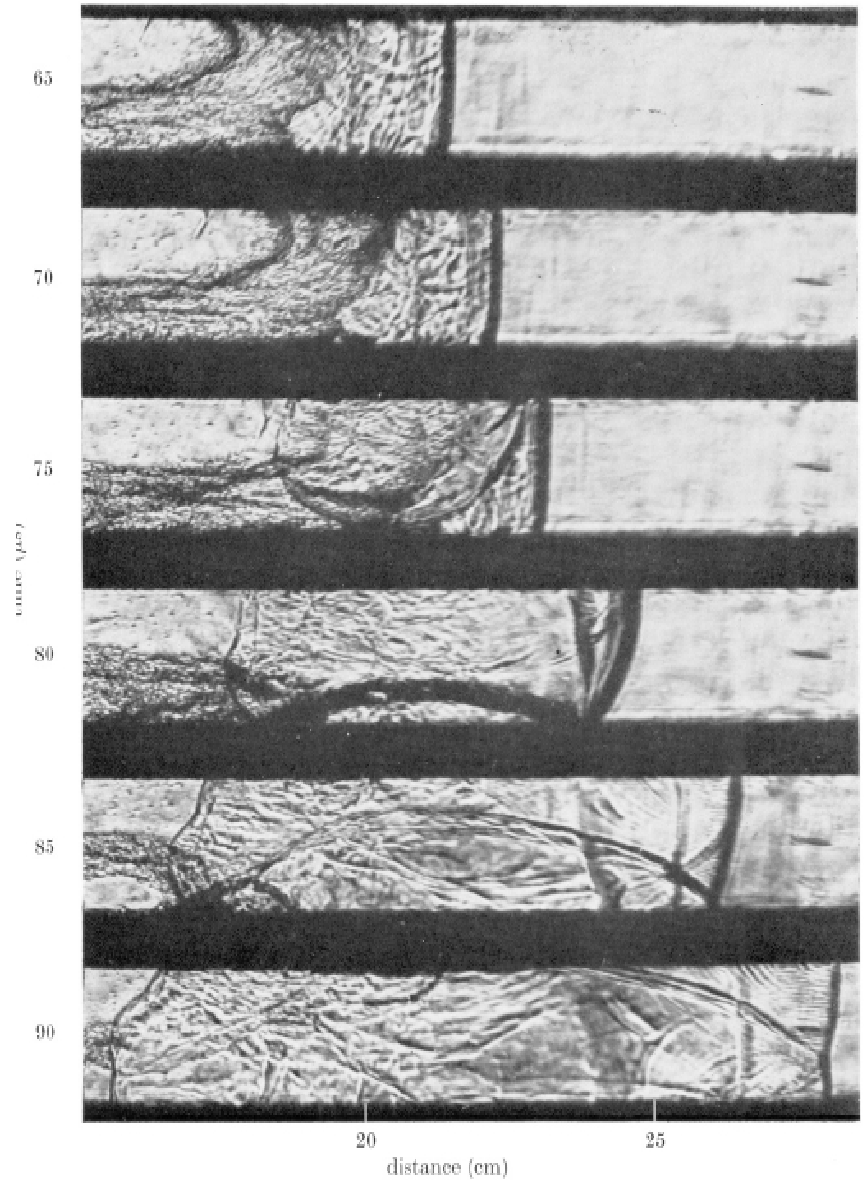

Figure 6(a). Enlargement of frames at 65 to 90 μs of figure 6.

Urtiev & Oppenheim 1965

Defalgration-to-detonation transition (DDT)

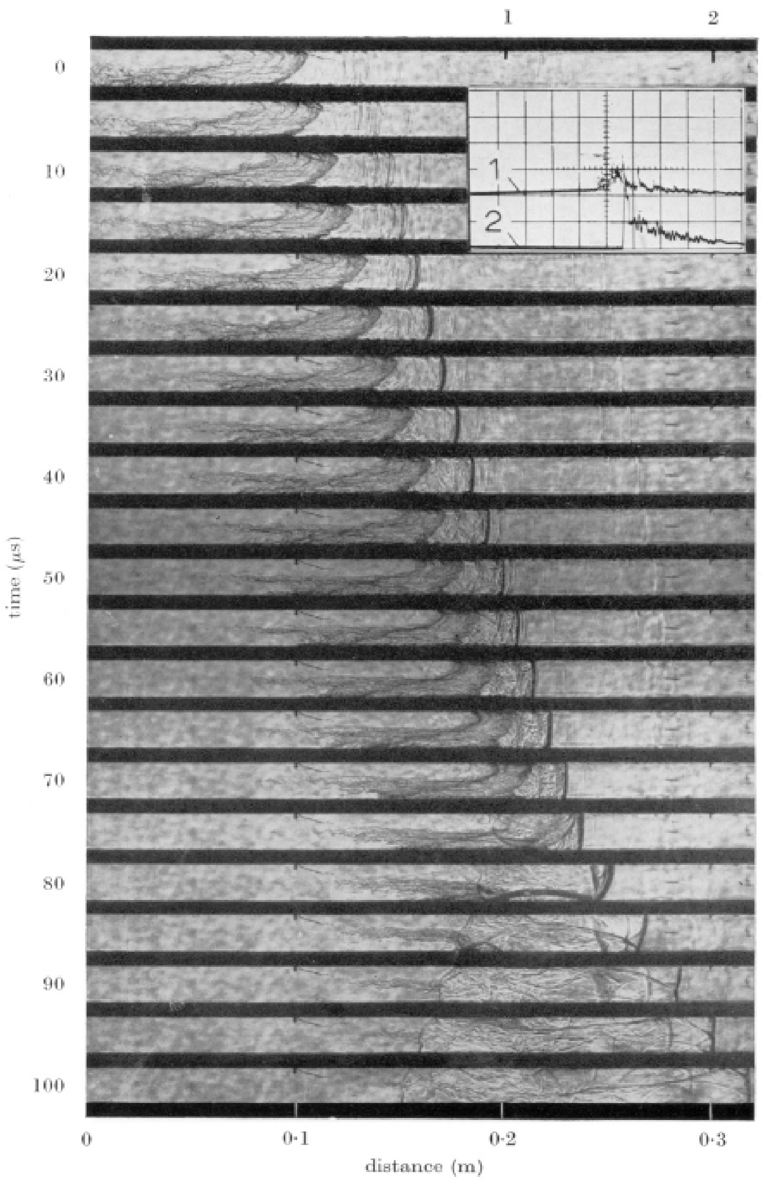

FIGURE 6. Stroboscopic schlieren record of the transition to detonation with onset between flame and shock. $2H_2 + O_2$ initially at a pressure of 554 mmHg. Pressure record shown in insert. Vertical scale: 1 division = 200 Lb./in.^{2}. Horizontal scale: 1 division = 50 μs. Oscilloscope sweep leads the photographic record by 180 μs.

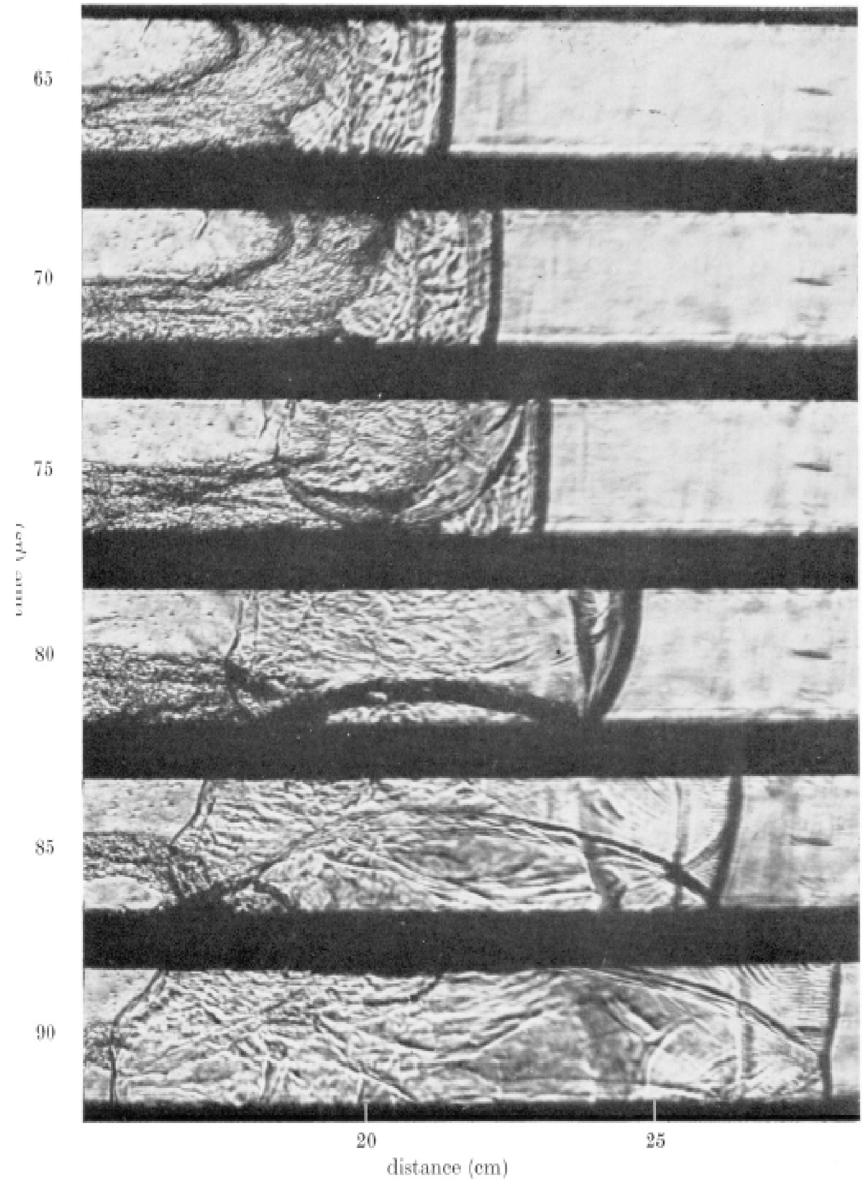

FIGURE 6(a). Enlargement of frames at 65 to 90 μs of figure 6.

Urtiev & Oppenheim 1965

Flame

Speed ~ 10 - 300 m/s
Overpressure ~ 1 – 10 (depends)

Detonation

Speed ~ 2 - 3 km/s
Overpressure ~ 40

DDT

Overpressure ~ 100
Time scale ~ 1 micro sec.

Big safety issues.

Project's goals:

- Fundamental understanding of flame acceleration and DDT

- First principle modeling of DDT in hydrogen-oxygen mixtures

- Predicting run distance to a detonation in long pipes

Code features

3D compressible reactive flow Navier-Stokes equations.

H_2+O_2 kinetics: 8 species, 19 reactions.

Multi-species NASA7 equation of state, temperature-dependent viscosity, heat conduction, mass diffusion, and radiation cooling.

Regular Cartesian mesh with cell-based AMR.

Dynamic mesh refinement and mesh re-balance every fourth time step.

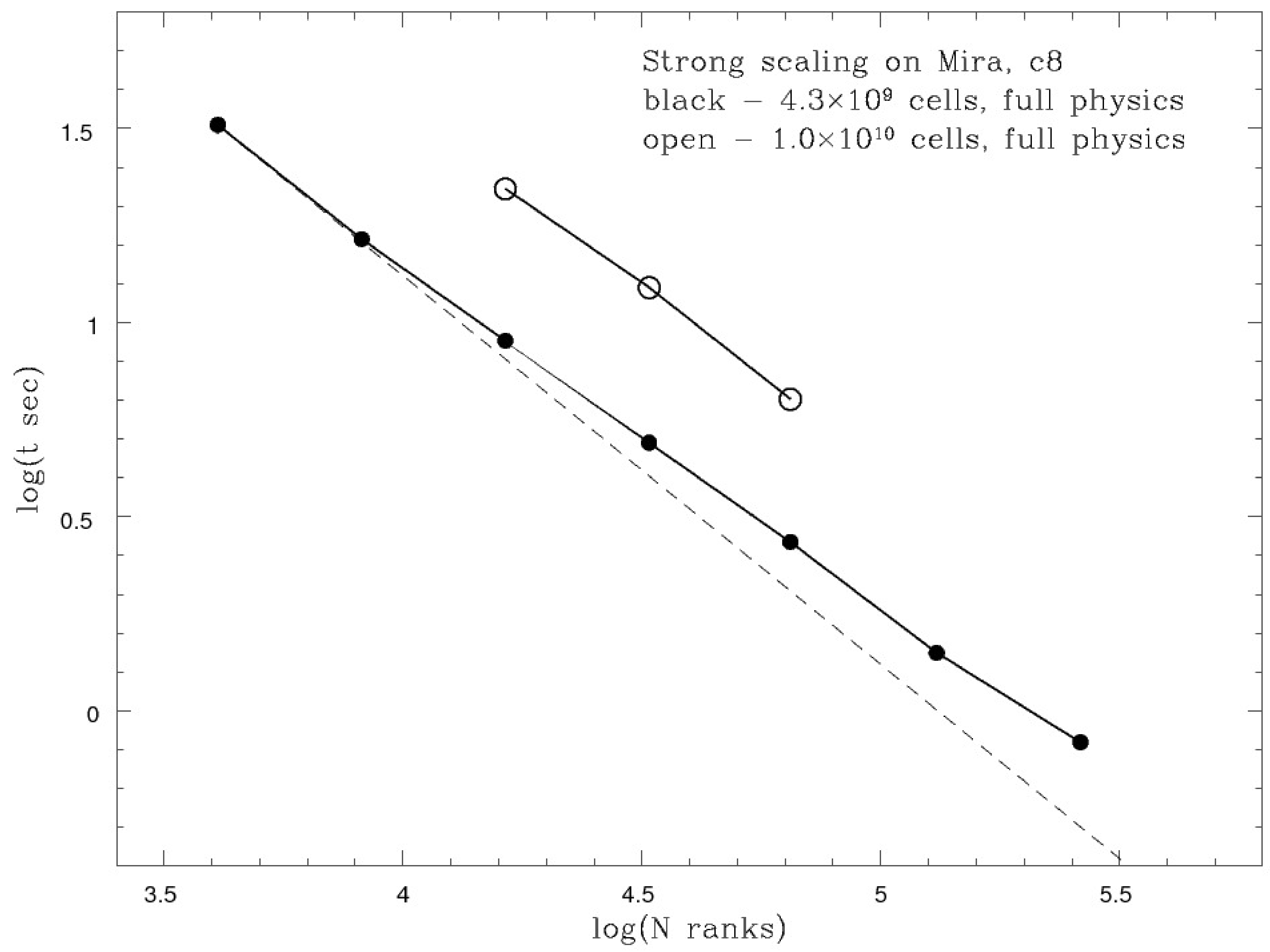
Strong scaling on Mira, c8
black – 4.3×10⁹ cells, full physics
open – 1.0×10¹⁰ cells, full physics
log(t sec)
log(N ranks)
1.5
1
0.5
0
3.5
4
4.5
5
5.5

$$\frac{\partial \rho}{\partial t} = -\nabla \cdot (\rho \mathbf{u}), \tag{1}$$

$$\frac{\partial \rho \mathbf{u}}{\partial t} = -\nabla \cdot (\rho \mathbf{u} \otimes \mathbf{u}) - \nabla P - \nabla \cdot \hat{\pi}, \tag{2}$$

$$\frac{\partial E}{\partial t} = -\nabla \cdot (\mathbf{u}\,(E + P)) - \nabla \cdot \mathbf{q}^{E}, \tag{3}$$

$$\frac{\partial \rho \mathcal{Y}_i}{\partial t} = -\nabla \cdot (\rho \mathbf{u} \mathcal{Y}_i) - \nabla \cdot \mathbf{q}^{d,i} + \rho \mathcal{R}_i, \quad i = 1, ..., N, \tag{4}$$

$$\hat{\pi} = -\mu \left((\nabla \mathbf{u}) + (\nabla \mathbf{u})^{T} - \frac{2}{3} \hat{\mathbf{I}} (\nabla \cdot \mathbf{u}) \right) \tag{5}$$

$$\mathbf{q}^{E} = \mathbf{u} \cdot \hat{\pi} - \lambda \nabla T + \sum_{i=1}^{N} H_i^0 \mathbf{q}^{d,i} \tag{6}$$

$$\mathbf{q}^{d,i} = \rho \mathcal{Y}_i \mathbf{u}^{d,i} \tag{7}$$

Kinetics

	Reaction	A, s^{-1}	n	E_a, kcal
1	$H + O_2 \leftrightarrows O + OH$	1.91×10^{14}	0.00	16.44
2	$O + H_2 \leftrightarrows H + OH$	5.08×10^{4}	2.67	6.292
3	$OH + H_2 \leftrightarrows H + H_2O$	2.16×10^{8}	1.51	3.43
4	$O + H_2O \leftrightarrows OH + OH$	2.97×10^{6}	2.02	13.4
5	$H_2 + M \leftrightarrows H + H + M$	4.57×10^{19}	-1.40	105.1
6	$O + O + M \leftrightarrows O_2 + M$	6.17×10^{15}	-0.50	0.00
7	$O + H + M \leftrightarrows OH + M$	4.72×10^{18}	-1.00	0.00
8	$H + OH + M \leftrightarrows H_2O + M$	4.50×10^{22}	-2.00	0.00
9	$H + O_2 + M \leftrightarrows HO_2 + M$	3.48×10^{16}	-0.41	-1.12
9a	$H + O_2 \leftrightarrows HO_2$	1.48×10^{12}	0.60	0.00
10	$HO_2 + H \leftrightarrows H_2 + O_2$	1.66×10^{13}	0.00	0.82
11	$HO_2 + H \leftrightarrows OH + OH$	7.08×10^{13}	0.00	0.30
12	$HO_2 + O \leftrightarrows OH + O_2$	3.25×10^{13}	0.00	0.00
13	$HO_2 + OH \leftrightarrows H_2O + O_2$	2.89×10^{13}	0.00	-0.497
14	$HO_2 + HO_2 \leftrightarrows H_2O_2 + O_2$	4.2×10^{14}	0.00	11.98
14a	$HO_2 + HO_2 \leftrightarrows H_2O_2 + O_2$	1.3×10^{11}	0.00	-1.629
15	$H_2O_2 + M \leftrightarrows OH + OH + M$	1.27×10^{17}	0.00	45.5
15a	$H_2O_2 \leftrightarrows OH + OH$	2.95×10^{14}	0.00	48.4
16	$H_2O_2 + H \leftrightarrows H_2O + OH$	2.41×10^{13}	0.00	3.97
17	$H_2O_2 + H \leftrightarrows H_2 + HO_2$	6.03×10^{13}	0.00	7.95
18	$H_2O_2 + O \leftrightarrows OH + HO_2$	9.55×10^{06}	2.00	3.97
19	$H_2O_2 + OH \leftrightarrows H_2O + HO_2$	1.0×10^{12}	0.00	0.00
19a	$H_2O_2 + OH \leftrightarrows H_2O + HO_2$	5.8×10^{14}	0.00	9.56

Table B.5: Lennard-Jones parameters, first 2 columns - [10], last two columns - [?]

Reactant	ϵ, ^{o}K	σ, Å	ϵ, ^{o}K	σ, Å
H	37.0	3.5	145.0	2.05
H_2	59.7	2.827	38.0	2.92
O	106.7	3.05	80.0	2.75
O_2	106.7	3.467	107.4	3.458
OH	79.8	3.147	80.0	2.75
H_2O	260.0	2.8	572.0	2.605
HO_2	106.7	3.467	107.4	3.485
H_2O_2	289.0	4.196	107.4	3.4558

where $T_l^* = T/\epsilon_l$ are the reduced temperatures, σ_l and ϵ_l are the Lennard-Jones cross-sections and potential parameters, respectively, and $\Omega^{(2,2)}$ is the dimensionless Lennard-Jones collisional integral given as a function of reduced temperature T^* in Appendix M-I of [9]. First two columns of Table B.5 give σ_s and ϵ_s adopted from Table 7-1 of [10]. Third and fourth columns give σ_s and ϵ_s taken from the GRI-Mech database [?].

Appendix B.3. Thermal conductivity

The coefficient of thermal conductivity of a mixture is [9–11]

$$\lambda = \sum_{l=1}^{N} \frac{\lambda_l \mathcal{Y}_l}{G_l^c}, \tag{B.7}$$

where

$$G_l^c = \sum_{k=1}^{N} \left(\delta_{lk} + \frac{1.065}{2\sqrt{2}} (1 - \delta_{lk}) \phi_{lk} \right) \mathcal{Y}_k \tag{B.8}$$

and

$$\lambda_l = E_l \lambda_l^0 \tag{B.9}$$

are the thermal conductivities of individual species corrected for the transfer of energy between translational and internal degrees of freedom. The uncorrected coefficients are

$$\lambda_l^0 = \frac{8.322 \times 10^3}{\sigma_s^2 \Omega^{(2,2)}(T_l^*)} \sqrt{\frac{T}{m_l}} = 3.12 \times 10^8 \frac{\mu_l}{m_l} \tag{B.10}$$

and the correction (Eucken) factors are

$$E_l = 1 + 0.354 \left(\frac{C_{p,l}^0}{R_g} - \frac{5}{2} \right). \tag{B.11}$$

Appendix B.4. Mass diffusion

Diffusion velocities $\mathbf{u}^{d,l}$ are determined by a system of Stefan-Maxwell diffusion equations combined with the condition on the zero total mass diffusion flux [9],

$$\sum_{k=1}^{N} \frac{m_l m_k \mathcal{Y}_l \mathcal{Y}_k}{D_{lk}} \left(\mathbf{u}^{d,k} - \mathbf{u}^{d,l} \right) = \mathbf{G}_l, \tag{B.12}$$

$$\rho \sum_{l=1}^{N} m_l \mathcal{Y}_l \mathbf{u}^{d,l} = \sum_{l=1}^{N} m_l \mathbf{q}^{d,l} = 0. \tag{B.13}$$

In Eq. (B.12)

$$\mathbf{G}_l = \nabla(\mathcal{M}\mathcal{Y}_l) - K_l^T \frac{\nabla T}{T} \tag{B.14}$$

are the combined gradients driving the diffusion of reactants where we take into account an ordinary mass diffusion and a seconday effect of thermal diffusion (Soret effect) which may be important for light species such as H and H_2,

$$D_{lk} = \frac{\mathcal{M}}{\rho} d_{lk}, \tag{B.15}$$

are binary diffusion coefficients, where

$$d_{lk} = \frac{2.265 \times 10^{-5}}{\sigma_{lk}^2} \left(\frac{m_l + m_k}{m_l m_k} \right)^{1/2} \frac{\sqrt{T}}{\Omega^{(1,1)}(T_{lk}^*)}, \tag{B.16}$$

and

$$K_l^T = \frac{\mathcal{M}}{R_g} \sum_{k=1}^{N} \frac{1.2\, C_{lk}^* - 1}{d_{lk}} \left(\frac{\mathcal{Y}_l m_l a_k - \mathcal{Y}_k m_k a_l}{m_l + m_k} \right), \tag{B.17}$$

are thermal diffusion ratios. Other variables are

$$\begin{aligned} \sigma_{lk} &= \frac{\sigma_l + \sigma_k}{2}, \quad a_l = \frac{\lambda_l^0}{G_l^c}, \\ C_{lk}^* &= \frac{\Omega^{(1,2)}(T_{lk}^*)}{\Omega^{(1,1)}(T_{lk})}, \quad T_{lk}^* = \frac{T}{\sqrt{\epsilon_l \epsilon_k}}, \end{aligned} \tag{B.18}$$

where $\Omega^{(1,1)}$ and $\Omega^{(1,2)}$ and dimensionless collisional integrals provided as a function of reduced temperature T^* in Appendix I-M of [9].

Following Giovangigli [12] we change variables in (B.12) from $\mathbf{u}^{d,k}$ to $\mathbf{q}^{d,k}$ and obtain a system of equations for diffusion fluxes

$$\sum_{k=1}^{N} \Gamma_{lk} \mathbf{q}^{d,k} = \mathbf{g}_l, \tag{B.19}$$

where

$$\begin{aligned} \Gamma_{lk} &= (1 - \delta_{lk}) \frac{\mathcal{Y}_l}{d_{lk}} - \delta_{lk} \sum_{k=1, k \neq l}^{N} \frac{\mathcal{Y}_k}{d_{lk}}, \\ \mathbf{g}_l &= \mathcal{M}^{-1} \mathbf{G}_l. \end{aligned} \tag{B.20}$$

Reflected shock tube experiments: shock bifurcation

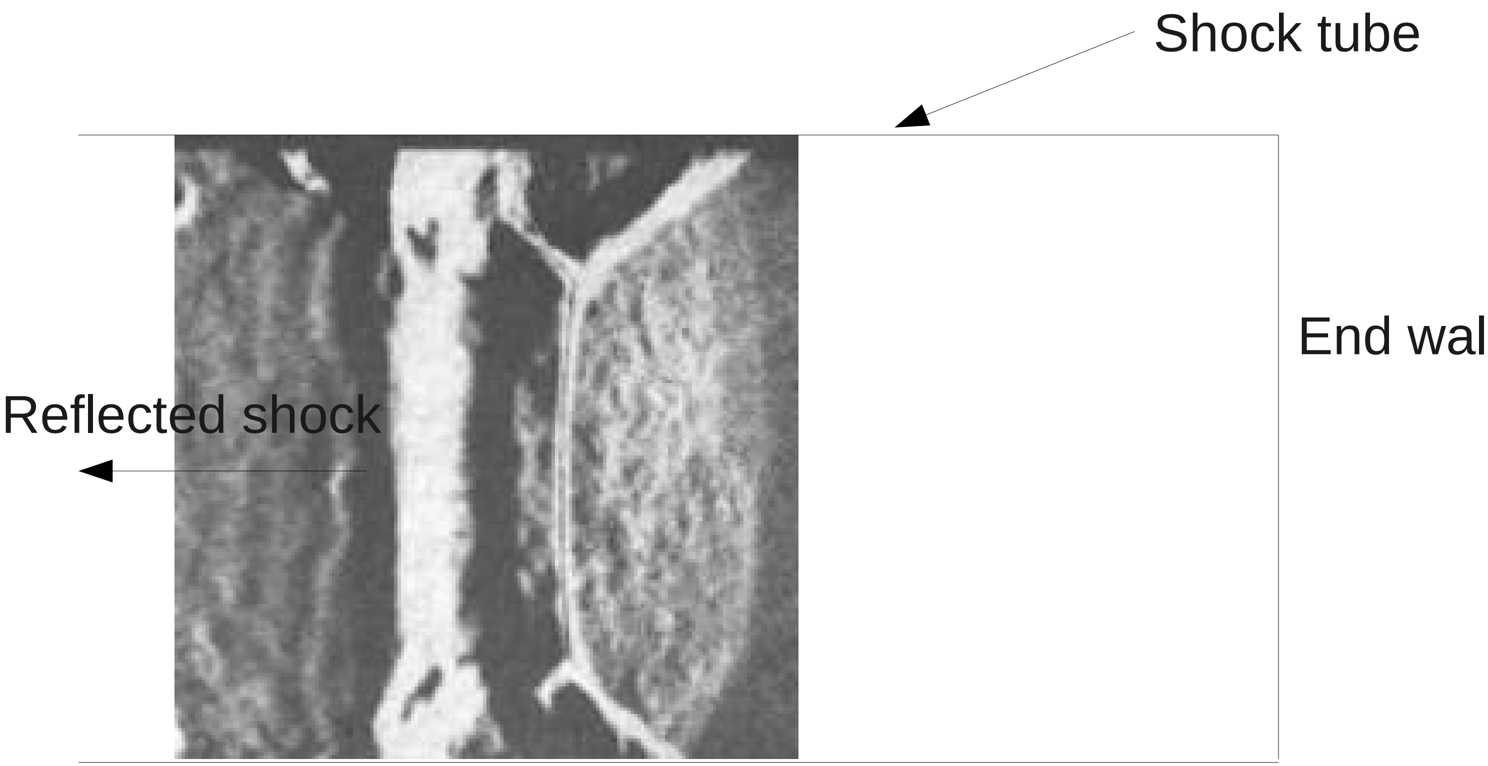

Brossard etal 1985

Reflected shock tube in CO2 validation

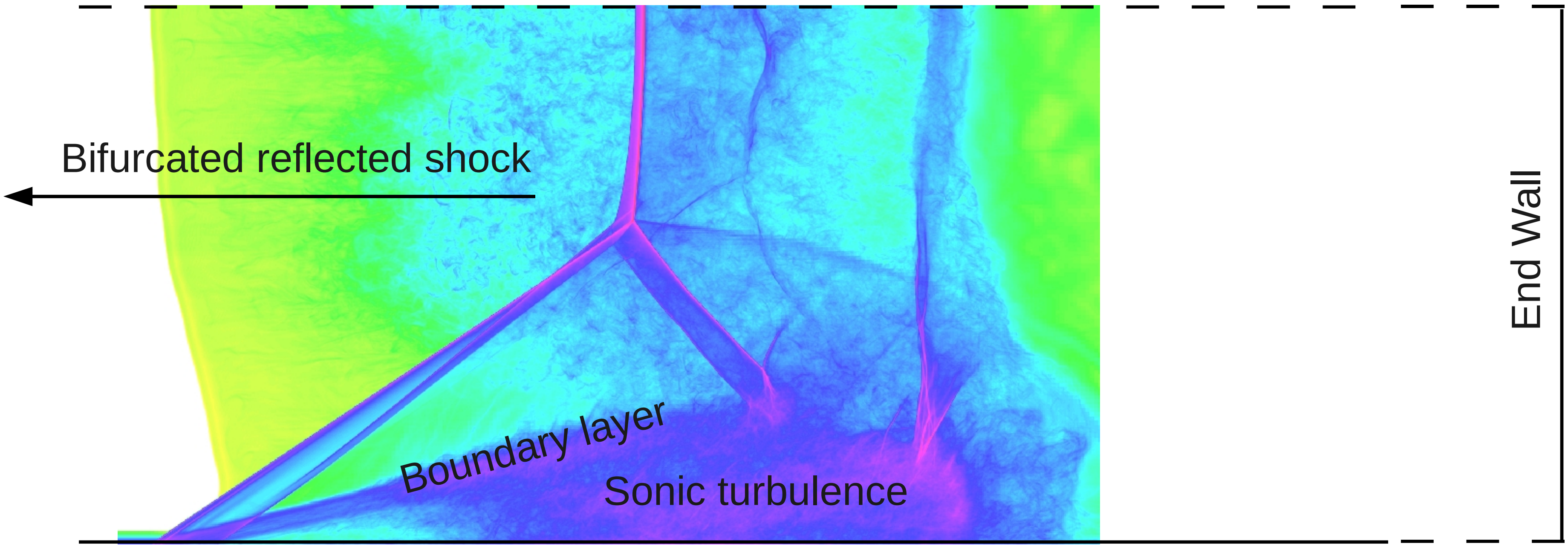

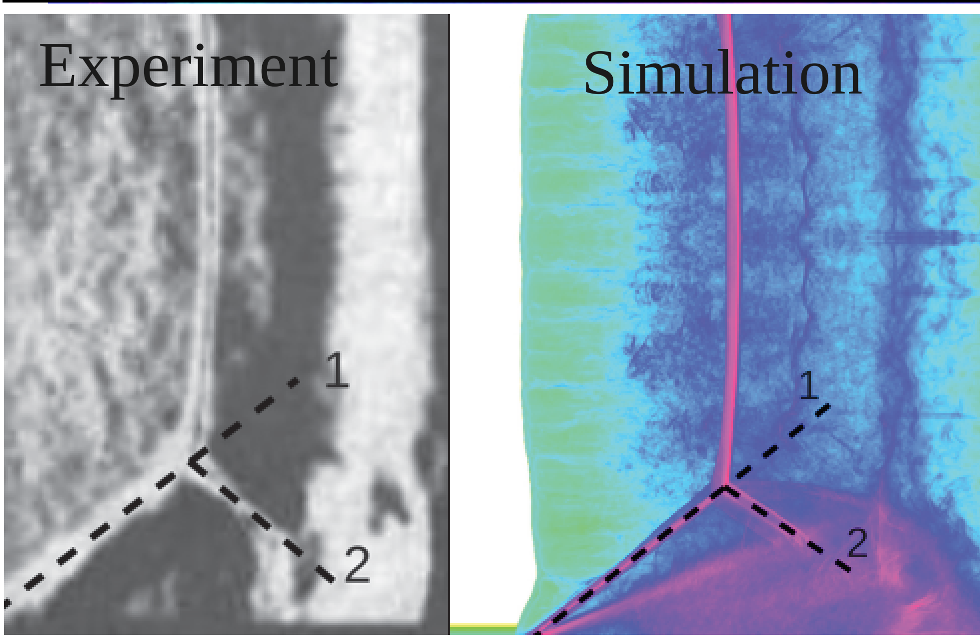

Comparison:

Angle	Experiment	Simulation
1	36 deg	37 deg
2	-128 deg	-124 deg

Reflected shock tube experiments
Simulation of strong ignition in $2H_2+O_2$

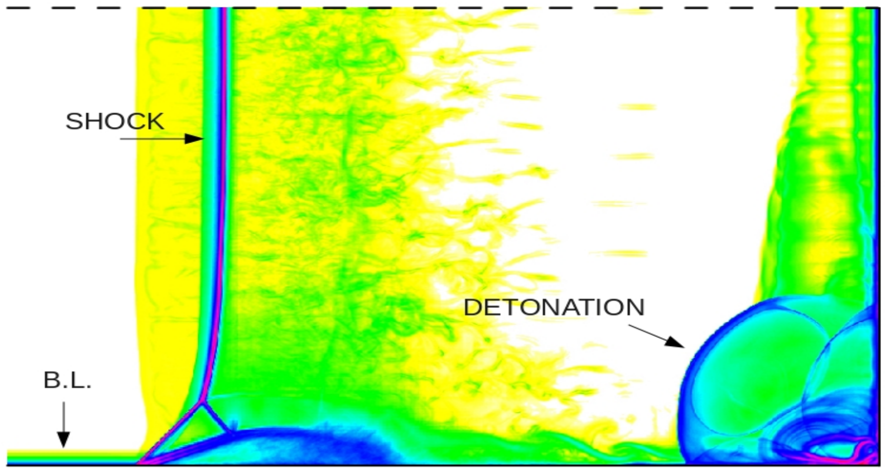

End wall

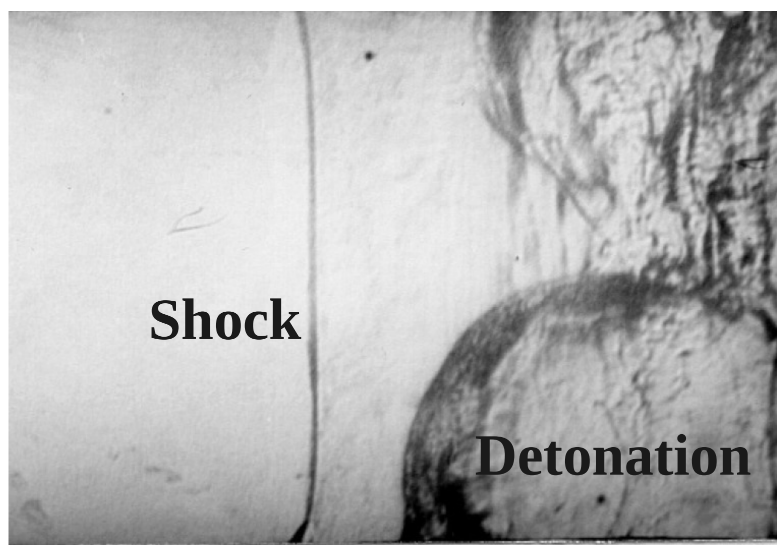

End wall

Reflected shock tube experiments: weak ignition

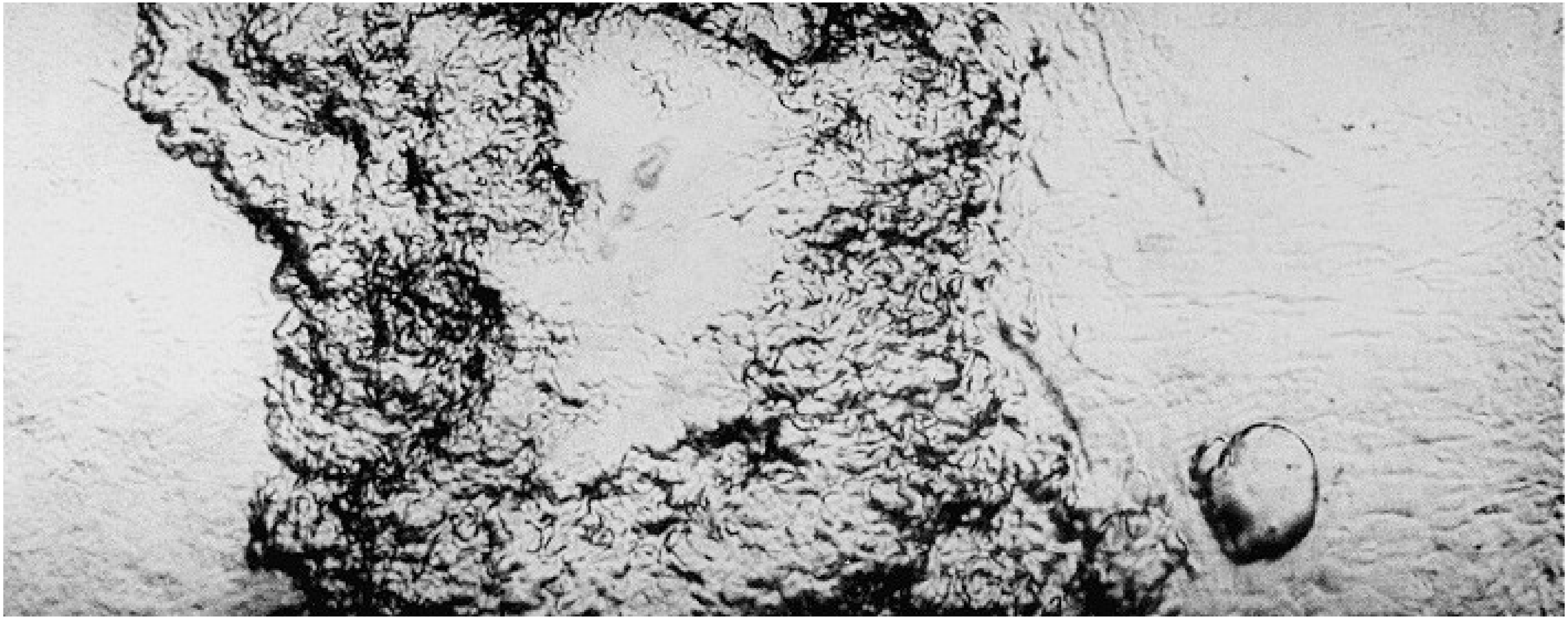

Thomas 2000

Reflected shock tube experiments
Simulation of weak ignition in 2H2+O2

Weak ignition in 2H2+O2, incident Mach number = 1.47

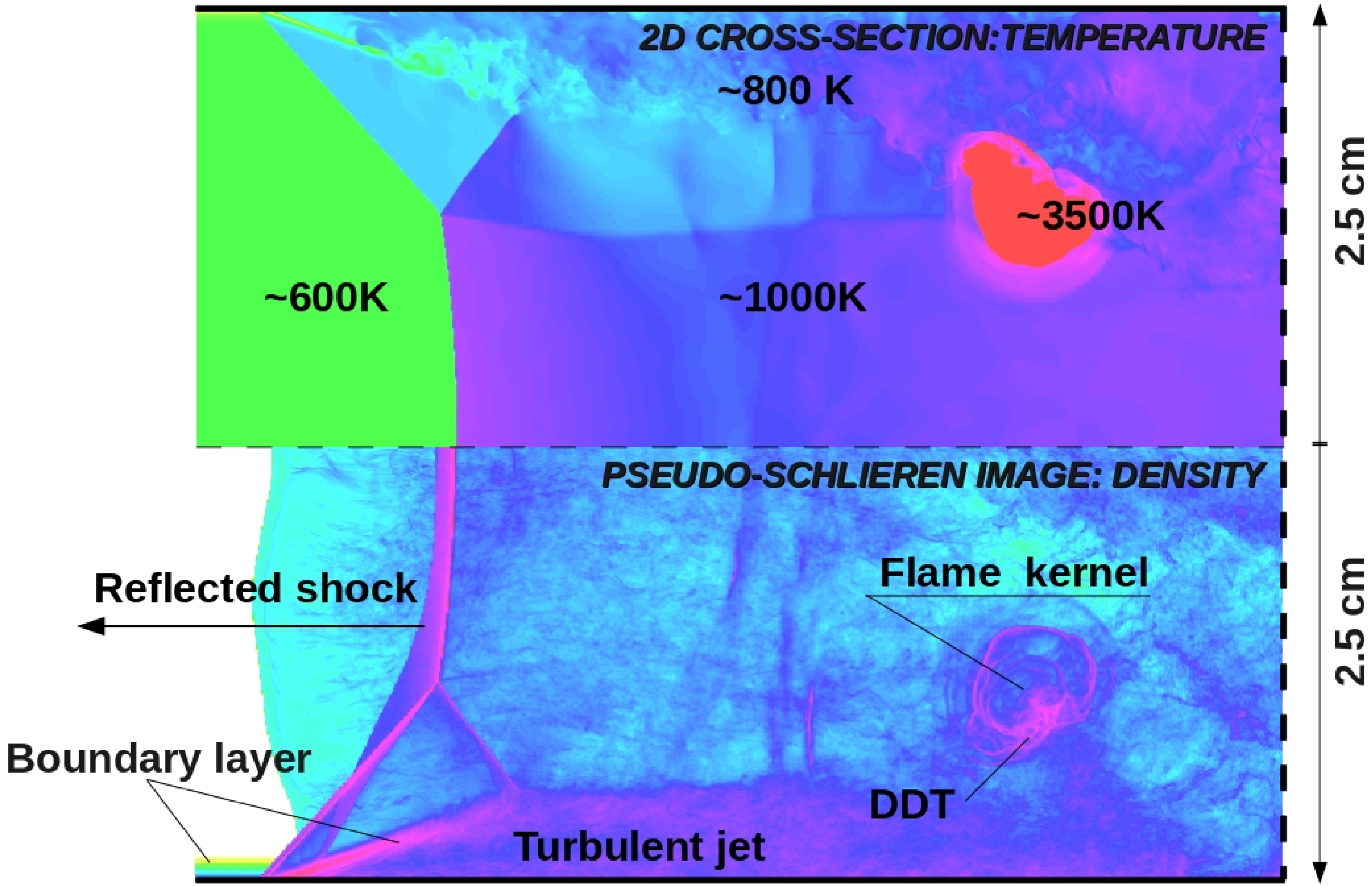

DDT in a hydrogen-oxygen mixture, BG/Q

DDT in 2H2+O2 at 1 atm. Initial pressure (schlieren)

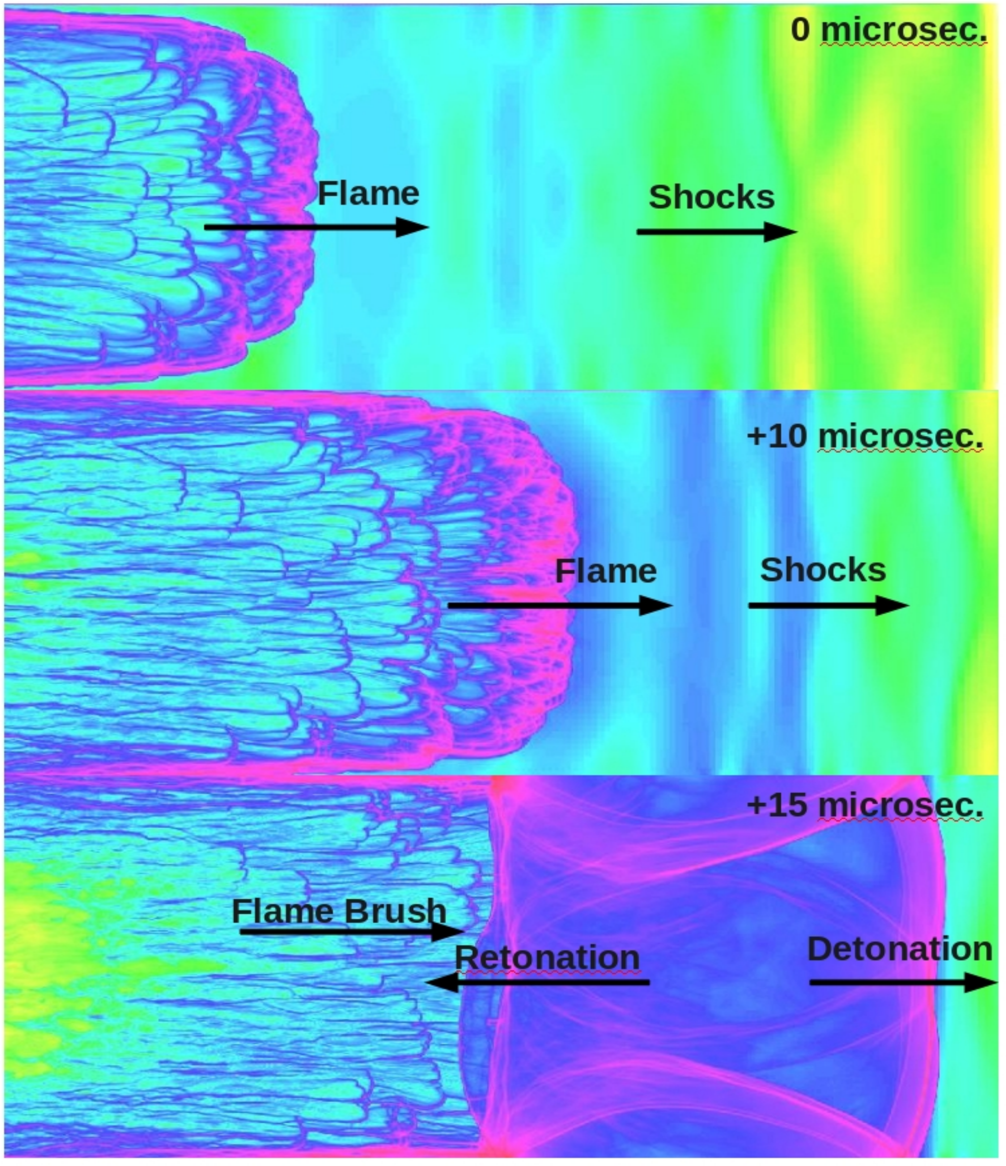

Next step: high resolution simulations of DDT in a long pipe.

Tube length 172 cm
Cross-section 2.7 cm x 2.7 cm
N cells ~ 10,000,000,000
N time steps ~ 50,000
Numerical resolution ~ 6 microns

Scaling plots, BG/P